

RENiO₃ single crystals (RE = Nd, Sm, Gd, Dy, Y, Ho, Er, Lu) grown from molten salts under 2000 bar oxygen-gas pressure

Yannick Maximilian Klein,^{*a} Mirosław Kozłowski,^b Anthony Linden,^c Philippe Lacorre,^d Marisa Medarde^{*a} and Dariusz Jakub Gawryluk^{*a}

a. Laboratory for Multiscale Materials Experiments, Paul Scherrer Institut, Forschungsstrasse 111, CH-5232 Villigen PSI, Switzerland.

b. Łukasiewicz Research Network - Tele & Radio Research Institute, 11 Ratuszowa Street, 03-450 Warsaw, Poland

c. Department of Chemistry, University of Zürich, Winterthurerstrasse 190, 8057 Zürich, Switzerland

d. Institut des Molécules et Matériaux du Mans (IMMM) - UMR 6283 CNRS, Le Mans Université, Avenue Olivier Messiaen, 72085 Le Mans, France

Corresponding author Emails: maximilian.klein@psi.ch; marisa.medarde@psi.ch; dariusz.gawryluk@psi.ch

ABSTRACT: The electronic properties of transition-metal oxides with highly correlated electrons are of central importance in modern condensed matter physics and chemistry, both for their fundamental scientific interest, and for their potential for advanced electronic applications. The design of materials with tailored properties has been, however, restricted by the limited understanding of their structure-property relationships, which are particularly complex in the proximity of the regime where localized electrons become gradually mobile. RENiO₃ perovskites, characterized by the presence of spontaneous metal-to-insulator transitions, are one of the most widely used model materials for the investigation of this region in theoretical studies. However, crucial experimental information needed to validate theoretical predictions is still lacking due to their challenging high-pressure synthesis, which has prevented to date the growth of sizable bulk single crystals with RE ≠ La, Pr and Nd. Here we report the first successful growth of single crystals with RE = Nd, Sm, Gd, Dy, Y, Ho, Er and Lu and sizes up to ~75 μm, grown from molten salts in temperature gradient under 2000 bar oxygen gas pressure. The crystals display regular prismatic shapes with flat facets, and their crystal structures, metal-insulator and antiferromagnetic order transition temperatures are in excellent agreement with previously reported values obtained from polycrystalline samples. The availability of such crystals opens access to measurements that have hitherto been impossible to conduct. This should contribute to a better understanding of the fascinating properties of materials with highly correlated electrons, and guide future efforts to engineer transition metal oxides with tailored functional properties.

INTRODUCTION

The properties of transition-metal oxides (TMOs) with correlated electrons at the boundary between localized and itinerant behaviour have fascinated the scientific community since the pioneering work of Mott in the early 1960's.¹ High temperature superconductivity, colossal magnetoresistance and metal-to-insulator transitions (MITs) are prominent examples of the exotic properties that can emerge in TMOs by approaching this region. Given their huge potential for applications in optoelectronics, data storage, neuromorphic and quantum computing technologies, understanding the origin of these properties is of fundamental importance for material design. However, the comprehension of the structure-property relationships in this kind of materials is less developed than in conventional semiconductors, where the electronic structure is well described by density-functional band theory and many functional characteristics such as the band-gap can now routinely be engineered.² One of the reasons for this is that state-of-the-art theoretical approaches only provide incomplete descriptions of the electronic and magnetic states in the presence of strong electronic correlations.³ But equally important is the scarcity of clean model systems (i.e., without chemical disorder or mixed-valence TMOs), which are crucial for comparing theoretical predic-

tions with experimental data. The nickelate perovskite family RENiO₃ (RE = trivalent *4f* lanthanide and Y³⁺) constitutes a unique, particularly well suited, and widely used system for this kind of investigations³⁻⁷ because, in contrast with most TMO systems, a complete evolution from a paramagnetic metal to an antiferromagnetic insulator can be realized without doping.⁸ LaNiO₃, the first member of the series, is paramagnetic, metallic and crystallizes in the rhombohedral $R\bar{3}c$ space group (SG).⁹⁻¹⁰ The remaining nickelates undergo spontaneous MITs at temperatures T_{MIT} that increase as the size of the RE-cation decreases, (Figure 1).¹¹⁻¹⁶ Long-range Néel order of the Ni magnetic moments has been observed at temperatures $T_N \leq T_{MIT}$, which coincide with the electronic localization in the case of PrNiO₃ and NdNiO₃ (Figure 1).^{10, 13, 17-22} RENiO₃ perovskites are thus intrinsically close to the boundary between localized and itinerant behavior, marked by the T_{MIT} vs RE radius line in Figure 1. This boundary can be crossed from both sides by changing either temperature, or the RE cation size (Figure 1), two clean, convenient variables for both, experimental and theoretical studies.

To date, most investigations on RENiO₃ nickelates have been focused on the mechanism at the origin of the MIT, which has been matter of an intense debate since its discovery in 1991.¹¹ The unusually high Ni oxidation state, formally Ni³⁺

low spin (LS) $t_{2g}^6 e_g^1$ and potentially Jahn-Teller active, suggested an electronic instability as a possible origin of the transition. On the other hand, the implication of the lattice has been confirmed by the giant ^{16}O - ^{18}O isotope effect on T_{MIT} ²³ and by diffraction studies, which revealed a subtle symmetry breaking from orthorhombic $Pbnm$ to monoclinic $P2_1/n$ below T_{MIT} that splits the unique Ni site of the high-temperature metallic phase into two inequivalent Ni sites with slightly different average Ni-O distances.^{15, 24-28} This breathing distortion, that contrasts with the expected deformation of the NiO_6 octahedra observed in other e_g^1 Jahn-Teller ions, has been interpreted as evidence of either a $2\text{Ni}^{3+} \rightarrow \text{Ni}^{3+\delta} + \text{Ni}^{3-\delta}$ charge disproportionation (CD),²⁴ or a Ni-O bond disproportionation with constant charge (2+) at the Ni sites and different amounts of holes at the O sites.²⁹ Concerning the role of magnetism, the situation is less clear, in particular because T_{MIT} and T_N do not always coincide. However, there is increasing evidence suggesting that the presence of the magnetically ordered state just below T_{MIT} may have an impact on the order of the transition.³⁰⁻³²

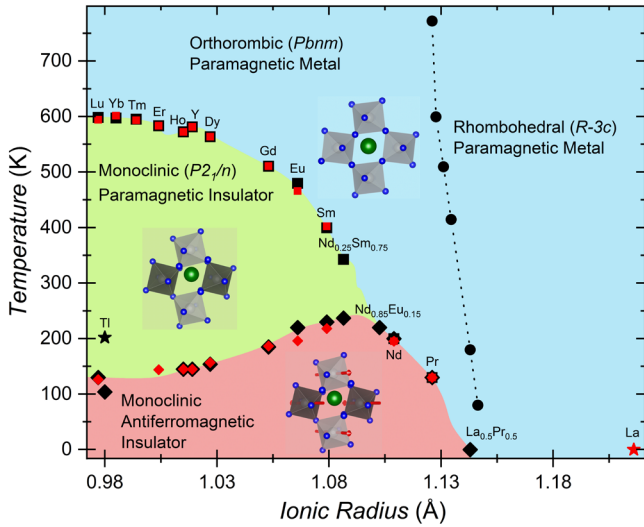


Figure 1. Phase diagram of bulk RENiO_3 perovskites. The red markers indicate the T_{MIT} (squares) and T_N (rhombuses) values obtained in this study. The black squares, rhombuses and circles are respectively the T_N , T_{MIT} and $Pbnm \rightarrow R3c$ structural transition values previously reported in the literature for bulk polycrystalline samples.^{10-22, 33} Red star: LaNiO_3 ($T_{MIT} = T_N = 0$ K). For nickelates with monoclinic $P2_1/n$ symmetry at base temperature, the ionic radii in the abscissa correspond with the values tabulated in Ref.³⁴ for trivalent $4f$ cations in 8-coordination. For rhombohedral LaNiO_3 with $R3c$ symmetry at base temperature, we use instead the ionic radii for trivalent $4f$ cations in 9-coordination.

The simultaneous presence of lattice, electronic and magnetic instabilities offers a unique opportunity to investigate the role of the three most relevant degrees of freedom that control the properties of most TMOs. At the same time, it makes a full understanding of the MIT mechanism a formidable task that challenges the state-of-the-art theoretical developments, such as Density-Functional³⁵ and Dynamical Mean-field Theory³⁶ methods. Ideally, the formalism and the

values of the fundamental interactions used in the calculations could be improved by comparing theoretical predictions with experimental data, in particular with the phonon, magnon, and electronic dispersion curves along different reciprocal space directions. However, this information is very limited due to the scarcity of nickelate single crystals. Although some band structures have been reported for nickelate thin films,^{37, 38} their properties differ in general from those of bulk samples due to their strong dependence on variables such as the film thickness or the lattice mismatch with the substrate. Moreover, thin films are not well suited for detailed diffraction studies, making difficult a detailed characterization of their crystal structures, which are needed as input in theoretical studies. A further limitation is that good quality epitaxial thin films have only been reported to date for the early nickelates ($\text{RE} = \text{La}$ to Eu), and just for a few substrate orientations.^{39, 40} Similar limitations also apply to magnon studies, where the available data are even scarcer, and only available for $\text{RE} = \text{Nd}$.^{41, 42} Phonon dispersions have not yet been reported, as far as we know. There is thus an urgent need for sizable, good quality bulk single crystals of the full nickelate series.

The reason behind the reduced single crystal availability has been the difficult synthesis procedure for bulk RENiO_3 perovskites, which require highly oxidizing conditions in order to stabilize the unusually high Ni formal valence (3+). The synthesis of the (nearly complete) RENiO_3 family ($\text{RE} = \text{Y}$, La , Nd , Sm , Eu , Gd , Ho , Er , Sm , Yb , Lu) was first reported by Demazeau et al. in 1971,¹⁹ who prepared them in polycrystalline form at 950°C and 60 kbar of hydrostatic pressure in a Belt apparatus by adding KClO_3 as an oxygen source. The nickelates with $\text{RE} = \text{Ce}$, Pr and Tb could not be stabilized under such elevated pressures due to the amphoteric character of these cations, which can display both, +3 or +4 oxidation states. Twenty years later, an alternative approach based in the use of much lower oxygen gas pressures (up to 200 bar) and high temperatures (1000°C) allowed Lacorre et al. to obtain PrNiO_3 for the first time.¹¹ NdNiO_3 , SmNiO_3 , EuNiO_3 and GdNiO_3 ^{11, 12, 43-46} could be also prepared in this way at slightly different temperatures using oxygen gas pressures up to 400 bar. This pressure was not enough to stabilize the nickelates with smaller RE cations (Dy to Lu), but Alonso et al.^{13, 14, 47} proved the possibility of synthesizing them at hydrostatic pressures (20 kbar) three times lower than those used by Demazeau, although in very small amounts (< 1 g). The syntheses were conducted in a piston-cylinder press at 900°C with KClO_4 as an oxygen source.

In line with the difficulties of preparing polycrystalline samples, obtaining good quality RENiO_3 single crystals has been to date extremely challenging. Attempts to growth PrNiO_3 and NdNiO_3 in different fluxes ($\text{KCl} / \text{NaCl} / \text{KClO}_4 / \text{NaClO}_4 / \text{NaOH}$) under high hydrostatic pressures (up to 40-45 kbar) and temperatures in the 1400-1500°C range have been reported in the past.⁴⁸⁻⁵⁰ Crystals up to 500 μm (Pr) and 100 μm (Nd) could be obtained, but they suffered from twinning due to the small deviations of their crystal structure from that of the cubic perovskite.⁵¹ Recently, large LaNiO_3 ^{52, 53} and PrNiO_3 ⁵⁴ single crystals were grown by the travelling solvent floating zone (TSFZ) technique under moderate oxygen

pressures (up to 150 bars). However, the oxygen stoichiometry was found to be inhomogeneous in both axial and radial growth directions⁵⁵. This had a huge impact on T_{MIT} and the magnetic behavior, very different from those reported for stoichiometric ceramic samples.

Here we report the first successful growth of $RENiO_3$ single crystals up to $\sim 75 \mu\text{m}$ in size for $RE = \text{Nd, Sm, Gd, Dy, Y, Ho, Er}$ and Lu with prismatic shapes, flat facets, and identical metal-insulator and antiferromagnetic transition temperatures to those of the polycrystalline samples of the same composition (Figure 1). We used an original method based in the use of moderate oxygen gas pressures (2000 bar), solvothermal growth in a temperature gradient, and highly reactive eutectic salt mixtures as fluxes that can be used to growth $RENiO_3$ nickelate crystals covering the full $4f$ series. The availability of such crystals will grant access to properties never reported to date for bulk samples. This should provide crucial insights to theoretical studies, contribute to a better understanding of the complex physicochemistry of correlated transition metal oxides, and pave the way to a targeted design of novel materials with strategically relevant magnetic and electronic properties.

RESULTS

High pressure crystal growth. The growth under such extreme conditions was carried out in a unique, non-commercial high oxygen gas pressure apparatus recently installed at the Paul Scherrer Institute (PSI) in Villigen, Switzerland.⁵⁶ As shown in Figure 2, the technical challenge of combining oxygen gas pressures up to 2000 bar with temperatures up to 1000°C is solved by minimizing the oxygen volume, whose pressure is continuously equilibrated by an inert gas (Ar) counter pressure. Another distinctive characteristic of the device is the large size of the main vessel ($\sim 50 \text{ cm}^3$), which allows solid state synthesis of ceramics, as well as solvothermal growth of single crystals, in large amounts.

For each nickelate, about 5g of nano-crystalline precursors were prepared by mixing stoichiometric amounts of rare earth RE_2O_3 and NiO (SI1, Materials and Methods), previously dried at 900°C and at 400°C , respectively. The mixed dehydrated oxides were dissolved in 75 ml of concentrated 65-75% HNO_3 (aq.). Water and nitric acid were removed by continuous stirring and heating the solution at 350°C . The solid residue was heated in a muffle furnace in air at 300°C for three hours, and the obtained black powder was further annealed at 650°C for 24 h in an alumina crucible under a 200 ml / min oxygen flow.

The resulting materials were mixed with a LiCl/KCl flux in a helium-filled glove box in the proportion 1:5 and placed into a semi-closed alumina reactor (internal diameter 11 mm and length 130 mm). For the flux, a eutectic mixture LiCl/KCl (4/6) was chosen for its relatively low melting point ($\sim 450^\circ\text{C}$), inert reactivity towards the $RENiO_3$ precursors and easy workup after the reaction (dissolves in water). An additional advantage is that it can play the role of an electrolyte, and thanks to that, the oxidation process can be boosted, increasing the kinetics and decreasing the thermodynamic parameters. The reactor was introduced into the high-pressure furnace (see scheme and picture in Figure 2) and heated up

to 850°C under 2000 bar oxygen gas pressure for 12 h. The temperature gradient between the bottom and top of the semi-closed reactor was $\sim 100^\circ\text{C}$. Under these conditions, phase pure $RENiO_3$ microcrystals with $RE = \text{Nd, Sm, Gd, Dy, Y, Ho}$ and Er could be obtained. To separate them from the

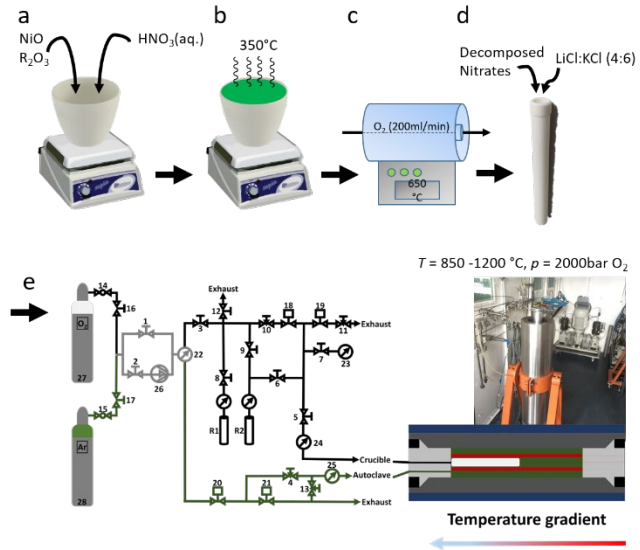


Figure 2. High-pressure single crystal growth process. (a) Dissolution of the starting oxides in nitric acid (65%, aq.); (b) evaporation of water and decomposition of NO_2/NO_3 ; (c) oxidation under O_2 flow; (d) mixing of precursors and solvent in a high pressure crucible; (e) schematic representation of the high-pressure, high-temperature furnace with the temperature gradient and Ar/O gas control setup (hand operated needle valves (1,-3, 5-9, 12, 16, 17); hand operated micro metering valves (4, 10, 11, 13); air operated valves (18-21); manometers (22-25); gas compressor (26); oxygen gas cylinder (27) with valve (14); argon gas cylinder (28) with valve (15); pressurised gas reservoirs (R1, R2)), together with a picture of the reactor.

flux, the final reaction products were washed with distilled water (to dissolve the LiCl/KCl eutectic), ethanol, and acetone, after which they were dried in air.

The nickelates with smaller rare earths ($RE = \text{Tm, Yb}$) could not be prepared in pure form using this procedure. As shown in Figure S1, large amounts of unreacted RE_2O_3 , NiO , REClO and/or mixed Li/Ni oxides were found to coexist with the $RENiO_3$ phases, which totalized $\sim 5\%$ of the final product' weight. Interestingly, the lattice parameters and T_{MIT} values of both, TmNiO_3 and YbNiO_3 were nearly identical to those reported in the literature (Figure S1). This suggested a kinetic origin for the incomplete $RENiO_3$ formation reaction, further confirmed by the increase of the TmNiO_3 weight fraction to $\sim 25\%$ after a second annealing (Figure S1b). In an attempt to speed up the process, a synthesis was performed for LuNiO_3 using a more oxidizing $\text{LiClO}_4/\text{KClO}_4$ (4/6) flux. Under the action of temperature and pressure the perchlorates decomposed, yielding the original LiCl/KCl (4/6) flux plus extra oxygen in the form of highly-reactive free radicals. After removing the flux, the final product contained phase-pure LuNiO_3 microcrystals ($\sim 90\%$ in weight), together with $\sim 10\%$ of unreacted Lu_2O_3 . Crystalline NiO and/or mixed Li/Ni oxides could not be observed, but they were probably present in nanocrystalline or amorphous form.

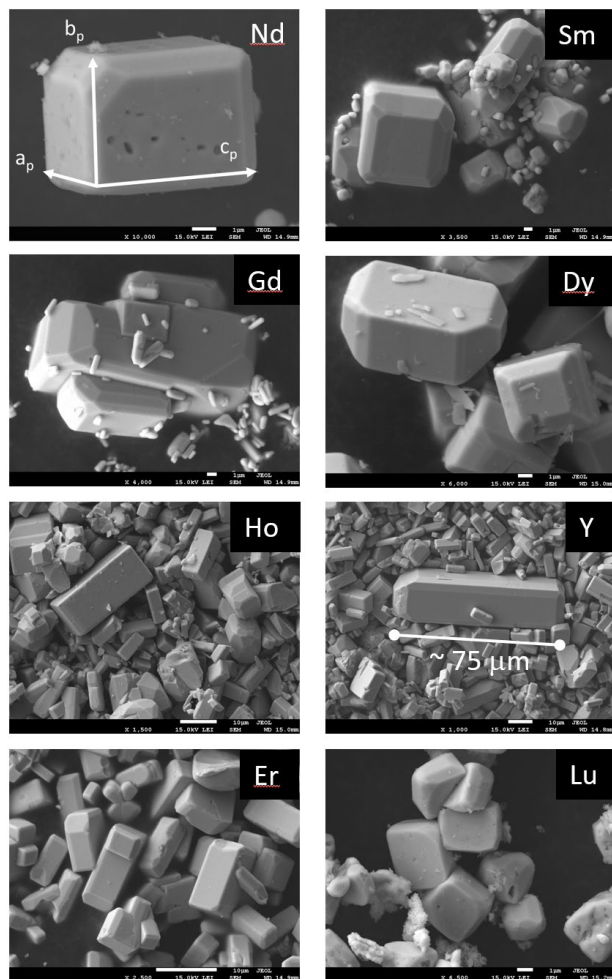


Figure 3 SEM images of the RENiO_3 microcrystals with RE = Nd, Sm, Gd, Dy, Y, Ho, Er and Lu. The most common facet orientation is illustrated for a NdNiO_3 crystal, where a_p , b_p and c_p denote the pseudocubic perovskite lattice parameters.

The single crystal nickelate set was completed with polycrystalline LaNiO_3 , PrNiO_3 , and EuNiO_3 samples. The PrNiO_3 and EuNiO_3 samples were the same used in our previous works,^{18, 32} where the synthesis route was already reported. LaNiO_3 was obtained by solid-state reaction at 950°C under 2000 bar oxygen pressure starting from the oxide precursors. The crystal habit, size and atomic composition of the crystals were characterized using Field-Emission Scanning Electron Microscopy (FE-SEM) coupled with Energy-Dispersive X-ray Spectroscopy (EDX). The phase purity and crystal structure of all samples were investigated by laboratory powder X-ray diffraction, plus single-crystal X-ray diffraction in the case of the larger crystals. Differential Scanning Calorimetry (DSC), SQUID magnetometry and Heat Capacity (C_p) were employed to characterize their physical properties and to determine their metal-insulator and antiferromagnetic order temperatures. Further details are provided in the Supporting Information.

Crystal habit, size and composition. The materials obtained after the flux removal had the appearance of fine powders, but examination under the optical microscope revealed tiny, well-separated microcrystals with sizes up to $\sim 75\ \mu\text{m}$. In spite of the increasing difficulty of stabilizing the RENiO_3

phases for the nickelates with smaller RE cations, the crystals were in general larger and more regular for YNiO_3 , HoNiO_3 and ErNiO_3 (Figure S2). These observations were confirmed by the SEM images (Figure 3), which revealed the presence of crystals with well-developed flat facets, most of them with a regular, truncated prism shape. This crystal habit was very different from that of the REClO phases present in some of the preparations and easily identifiable owing to their characteristic diamond-like shape (Figure S3). The chemical composition of the crystals (REClO and RENiO_3) was checked by EDX, which confirmed the nominal stoichiometry (Figures S3 and S4).

The facet orientation of the RENiO_3 phases was checked for some of the largest exemplars using single-crystal X-ray diffraction. In most of them, the largest crystal facets were perpendicular to the pseudocubic perovskite crystal axes a_p and b_p , with the longest edge parallel to the $c = 2a_p$ axis of the orthorhombic $Pbnm$ unit cell, as shown in Figure 3. The $a = a_p - b_p$ and $b = a_p + b_p$ $Pbnm$ axes, parallel to the in-plane diagonals of the pseudocubic perovskite cell, were thus perpendicular to the truncated facets. Well-developed facets were in general not observed in crystals with sizes smaller than $0.5\ \mu\text{m}$. Recrystallization attempts aimed at increasing the nickelate crystal size were conducted in the case of SmNiO_3 by repeating the growth procedure, but they were unsuccessful. Instead, larger amounts of SmClO were observed, with crystal sizes notoriously larger than in the original preparation (Figure S5). We do not exclude that larger nickelate crystals can be prepared in the future, but this will require additional experimental work.

Crystal structure. As mentioned in the introduction, all nickelates in polycrystalline form, with the exception of LaNiO_3 , feature sharp MITs with pronounced anomalies in the lattice parameters. However, the subtle $Pbnm \rightarrow P2_1/n$ symmetry-breaking below T_{MIT} and the associated splitting of the Ni sites has only been reported for some members of the family (RE = Pr^{25} , Nd^{28} , Sm^{27} , Dy-Lu^{15, 16, 26}). The reason behind this is the smallness of the monoclinic angle β , that at RT takes values between $\sim 90.16^\circ$ (Lu)⁴⁷ and $\sim 90.04^\circ$ (Sm)²⁷ - NdNiO_3 and PrNiO_3 are metallic and orthorhombic at RT, and is thus difficult to detect with standard laboratory X-ray diffraction techniques. Only high resolution powder diffraction (neutron or X-ray synchrotron) was able to reveal the tiny monoclinic distortion and the associated splitting of the Ni sites in the insulating state, whose crystal structure was described as orthorhombic $Pbnm$ in early studies at both sides of the MIT. Although the existence of a monoclinic distortion below T_{MIT} has not yet been reported for EuNiO_3 and GdNiO_3 , evidence supporting a direct link between the MIT and the existence of two distinct Ni sites in the insulating state for the whole RENiO_3 family has been provided by other techniques, such as X-ray absorption⁵⁷ and Mössbauer spectroscopies.^{16, 26}

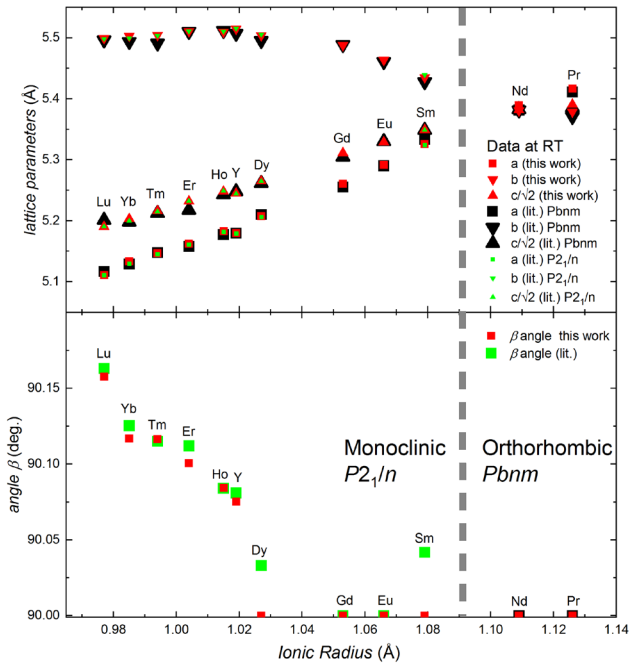


Figure 4. RT lattice parameters a , b and c and β of $RENiO_3$ perovskites as a function of the RE ionic radius. The red markers are the values obtained in this study. The remaining markers are data reported in the literature for ceramic samples using the $Pbnm$ (black)¹⁹ and $P2_1/n$ (green)^{26, 28, 47} groups.

This scenario is also supported by most theoretical studies,^{4, 6, 7, 58, 59} where the presence of small and large NiO_6 octahedra

emerges as the main distinctive characteristic of the insulating phase, as well a necessary condition for the electronic localization below T_{MIT} .

The results of the structural characterization of our nickelate samples fully agrees with this picture for both ceramics (RE = La, Pr and Eu) and single crystals. As shown in Figure S6, the laboratory powder X-ray diffraction patterns of $LaNiO_3$, $PrNiO_3$ and $NdNiO_3$ could be indexed on the basis of a rhombohedral $R\bar{3}c$ (La) or an orthorhombic $Pbnm$ lattice (Pr and Nd), in agreement with previous studies. For $SmNiO_3$ and $DyNiO_3$, reported to be insulating and monoclinic at RT the tiny angle β reported in previous works ($\sim 90.04^\circ$ ²⁷ and $\sim 90.03^\circ$ ²⁶, respectively) could not be resolved by our laboratory equipment. This was also the case for $EuNiO_3$ and $GdNiO_3$, where the existence of a monoclinic distortion has not been reported to date. A clear splitting of the (hkl) and $(-hkl)$ reflections consistent with a monoclinic angle $\beta \neq 90^\circ$ was, in contrast, clearly observed for $YNiO_3$, $HoNiO_3$, $ErNiO_3$, $TmNiO_3$, $YbNiO_3$ and $LuNiO_3$, which were reported to be insulating and monoclinic at RT with substantially larger β angles. The Rietveld fits, shown in Figures S1 and S6, were thus conducted with the SG $Pbnm$ for the nickelates with RE = Pr, Nd, Sm, Eu, Gd and Dy, and with $P2_1/n$ for those with RE = Y, Ho, Er, Tm, Yb and Lu. However, the observation of MITs with transition temperatures nearly identical to those reported in the literature for all nickelates with $R \neq La$ (see Figure 1 and the section “metal insulator transitions”) strongly suggest that $SmNiO_3$, $EuNiO_3$, $GdNiO_3$ and $DyNiO_3$ are actually monoclinic at RT.

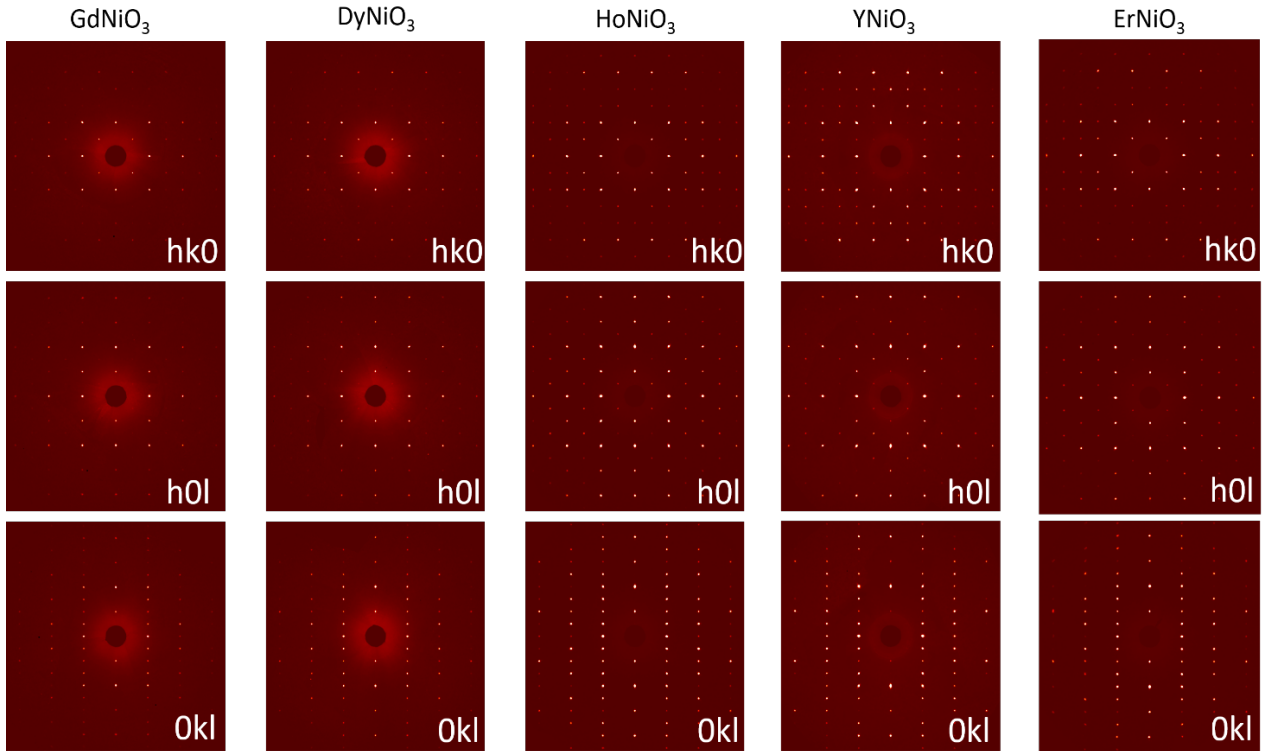


Figure 5. Reciprocal (hko) , (hol) and (okl) lattice planes measured by laboratory X-ray diffraction (Mo $K\alpha$) at RT for nickelate single crystals with RE = Gd, Dy, Ho, Y and Er, illustrating the agreement between the observed systematic absences and those of $Pbnm$.

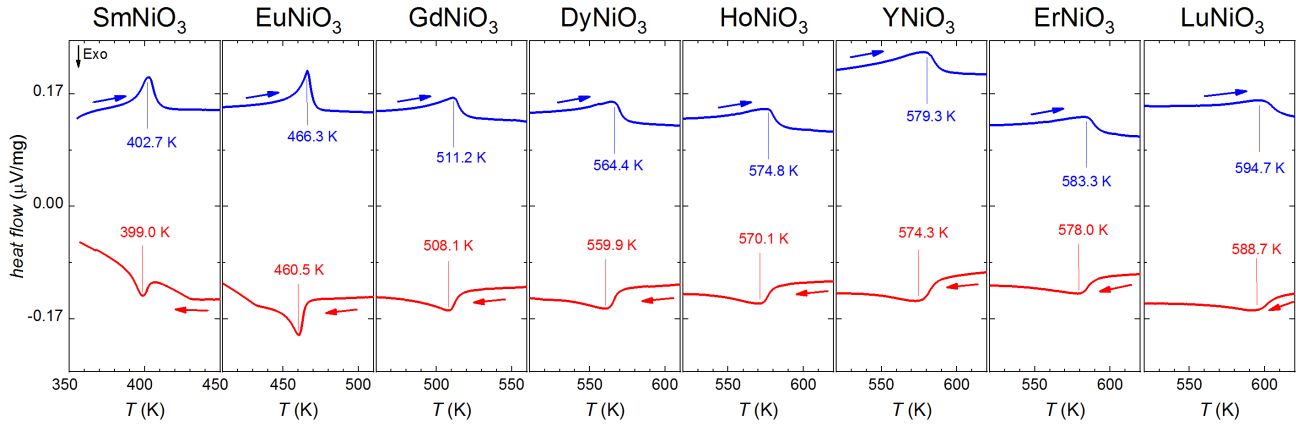


Figure 6. DSC curves obtained for the RENiO_3 single crystals (RE = Sm, Gd, Dy, Y, Ho, Er and Lu) and polycrystalline EuNiO_3 in a heating/cooling cycle.

The refined structural parameters, interatomic distances, and angles, very similar those reported in previous studies, are summarized in Table S1. The excellent agreement is illustrated in Figure 4, where the a , b , c and β lattice parameters of our samples (red symbols) are compared with those of refinements performed using the $Pbnm$ and $P2_1/n$ SGs (black and green symbols, respectively).

The powder diffraction data were complemented with laboratory single-crystal X-ray diffraction data sets for the best, untwined exemplars (see the SI for further details on data collection and analysis). The highly single crystalline quality of representative GdNiO_3 , DyNiO_3 , YNiO_3 , HoNiO_3 and ErNiO_3 specimens is illustrated in Figure 5, showing selected high-symmetry reciprocal lattice planes reconstructed from the RT data sets. The lattice metrics were compatible with the mmm Laue class and the systematic absences consistent with those of $Pbnm$ for the five nickelates, including those whose monoclinic symmetry at RT was confirmed by PXRD. This was an expected result given the smallness of the monoclinic distortion and the superior 2θ resolution of powder diffractometers, which are better suited than single crystal diffractometers for the determination of the lattice geometry. Their crystal structures were thus refined using $Pbnm$. The obtained structural data, summarized in the deposited CIF files, are consistent with those obtained from the powder diffraction data (see the SI for further details and for the Cambridge Crystallographic Data Centre deposition numbers). The crystal structures of the five nickelates together with the associated atomic displacement ellipsoids (50 % probability) are shown Figure S7.

For NdNiO_3 , SmNiO_3 and LuNiO_3 , crystal sorting, mounting, data collection and analysis were more challenging. This was due to their smaller crystal size (Figure 3), the presence of impurities (RE = Lu) and in the case of RE = Nd and Sm, to the frequent presence of twins. An in depth single-crystal diffraction investigation of these three nickelates will require additional experimental work and will be presented separately.

Metal-to-insulator transitions. Besides diffraction data, a central parameter for assessing the match between the properties of our crystals and those of previously reported ceramic samples is the value of the metal-insulator temperature T_{MIT} . For the nickelates with the smallest rare earth ions (RE = Sm, Eu, Gd, Dy, Y, Ho, Er and Lu), where the metal to insulator transition was reported to occur above 400K, T_{MIT} was determined using DSC. This technique, also employed in refs.^{12, 13, 15, 23}, was used instead of resistivity measurements for two reasons: the T_{MIT} values were above the operation limit of our equipment (a PPMS 9T with $T_{max} = 400$ K), and the largest RENiO_3 single crystals, too small to be contacted manually, could not be pressed or sintered to form dense pellets. DSC can easily access the required temperature range ($400\text{K} < T < 600\text{K}$), and provides a direct measurement of the enthalpy (H) change at the metal-to-insulator transition. This is related to the heat capacity at constant pressure (C_p) through the relationship $C_p = \frac{1}{m} \left(\frac{\partial H}{\partial T} \right)_p = \frac{1}{m} \frac{\Delta P}{\beta}$, where m is the sample mass, β is the heating rate $\partial T/\partial t$ during the DSC measurement, and ΔP is the absolute value of the heat flow through the sample (i.e., the absolute value of the DSC signal). Above 400K, the electronic and magnetic contributions to C_p are in general very small, and the largest contribution comes from the lattice. Since the MIT in nickelates is also a first-order structural transition involving a SG change and pronounced discontinuities in the lattice parameters, it gives rise to an anomaly in the C_p that can be easily detected in the DSC signal.

Figure 6 shows the DSC signals measured by heating (in blue) and cooling (in red) of these nickelates, confirming the presence of endothermic peaks in the heating curves, with maxima between 402.7 K (Sm) and 594.7 K (Lu). These values, plotted as red symbols in Figure 1 and summarized in Table S2, are nearly identical to the metal-insulator temperatures reported in the literature and obtained using different techniques (black symbols in Figure 1). The exothermic peaks observed in the cooling curves display maxima at temperatures a few degrees lower, which indicate the presence

of hysteresis. This behavior, characteristic of first order transitions, has been observed at T_{MIT} for all nickelates, further supporting the assignment of the DSC peaks to the MIT's.

For PrNiO_3 (already reported in our previous study³²) and NdNiO_3 , where the electronic and magnetic transitions coincide, $T_{MIT} = T_N$ was determined from bulk magnetic susceptibility $\chi = M/\mu_0 H$ measurements (Figure 7). For both nickelates, the $\chi(T)$ curves are dominated by the paramagnetic contribution of Pr^{3+} and Nd^{3+} , with nominal $\mu_{\text{eff}} = 3.58$

and $3.62 \mu_B$ values, respectively (Table S3). However, tiny anomalies at 130.1 K (Pr) and 196.2 K (Nd), better appreciated in the $1/\chi$ curves, are clearly observed. As shown in Figure 1, these values agree very well with those previously reported from neutron diffraction.

Magnetic transitions. Complementary to T_{MIT} , the antiferromagnetic ordering temperatures of the Ni and RE

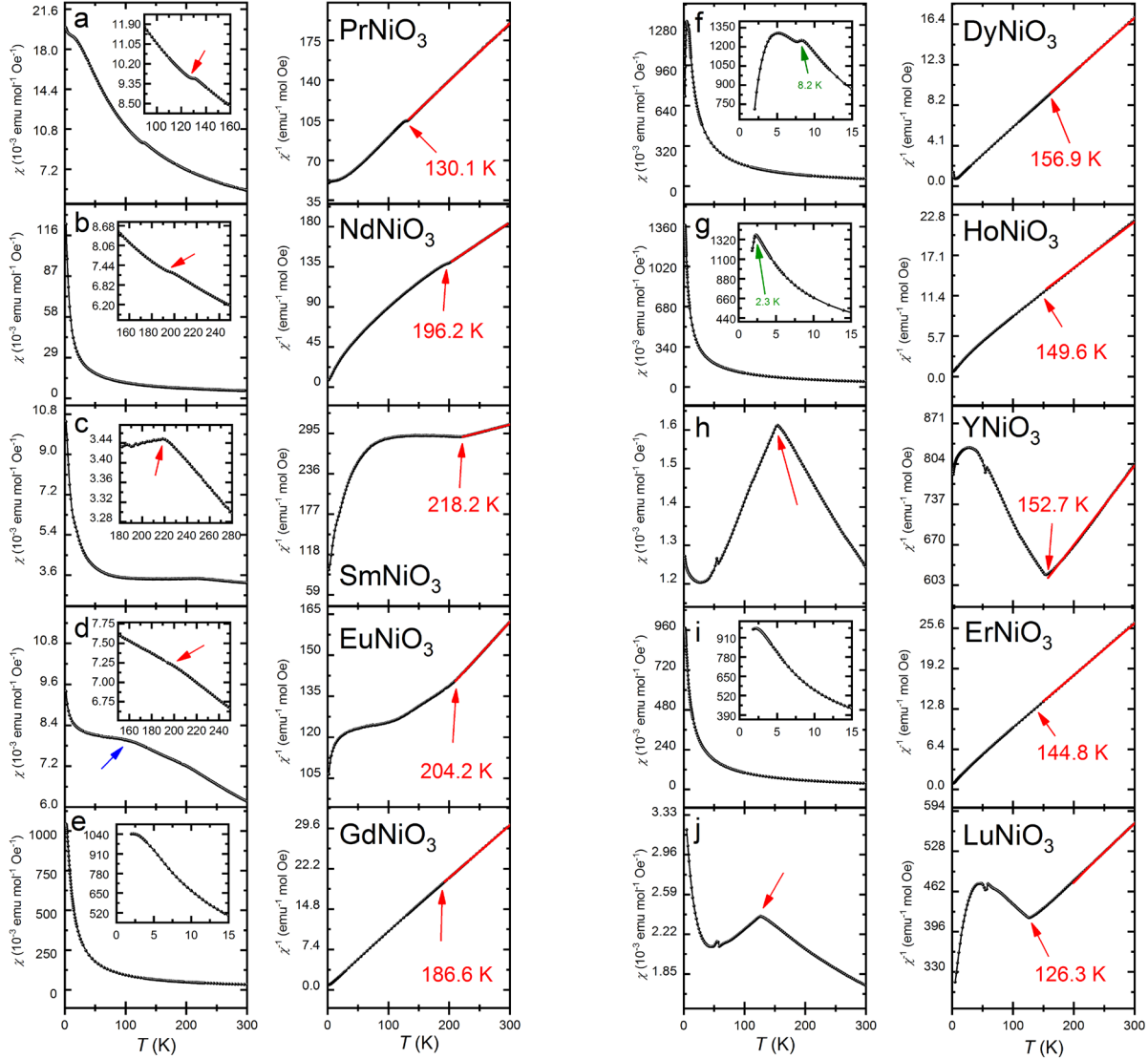


Figure 7. Temperature dependence of the magnetic susceptibility and its inverse, as obtained for our RENiO_3 single crystals (RE = Nd, Sm, Gd, Dy, Ho, Y, Er, Lu) and ceramics (RE = Pr, Eu). The red arrows indicate the antiferromagnetic ordering temperature T_N of the Ni sublattice and the green arrows in (f) and (g) those of the Dy and Ho sublattices. The blue arrow indicates the inflexion point associated to the van Vleck paramagnetic signal in EuNiO_3 . The Red lines indicate the temperature range used for the Curie-Weiss fits. The Pr data are from Ref.³²

sublattices offer an additional way to assess the properties of our crystals. We thus performed additional magnetic susceptibility measurements for the nickelates with $\text{RE} \neq \text{Pr, Nd}$, where T_N and T_{MIT} are well separated and T_N is expected to be below RT. As shown in Figure 7, clear anomalies in the $\chi(T)$ and $1/\chi(T)$ curves could be observed for SmNiO_3 (218.2 K), EuNiO_3 (204.2 K), YNiO_3 (152.7 K) and LuNiO_3 (126.3 K), very similar to those reported in previous studies on powder

samples (Figure 1). For the nickelates with $\text{RE} = \text{Gd, Dy, Ho}$ and Er , no anomaly was evident in the $\chi(T)$ curves due to the huge paramagnetic contribution of the RE^{3+} magnetic moments, which mask the weak signal of the Ni sublattice. The T_N values were thus determined from heat capacity (C_p) measurements as a function of temperature, as shown in Figure 8. Tiny peaks at $T = 186.6$ K, 156.9 K and 149.6 K are clearly observed for GdNiO_3 , DyNiO_3 and HoNiO_3 , respectively, and

are very similar to the T_N values reported in refs.^{13,20}(Figure 1). For ErNiO_3 , where an experimental T_N value has not been reported so far, a similar anomaly is observed at 144.8 K, very close to the extrapolated T_N value reported in ref.⁸.

For DyNiO_3 and HoNiO_3 , additional anomalies with sharp maxima at $T \sim 8.2$ K and ~ 2.3 K were observed in the $\chi(T)$ curves. These values are very similar to the long-range ordering temperatures of the Dy^{3+} and Ho^{3+} magnetic moments determined by neutron powder diffraction^{20,26}, further confirming the excellent agreement between the physical properties of our samples and those of previously reported powder samples.

Effective paramagnetic moments and Curie-Weiss temperatures. Although an in-depth characterization of the RE and Ni magnetism in RENiO_3 perovskites is out of the scope of this work, the analysis of the inverse magnetic susceptibility $1/\chi$ in the paramagnetic region ($T > T_N$, see Figure 7 and the SI for details) provides a first hint about the sign and size of the dominant magnetic interactions and the effective paramagnetic moments μ_{eff} along the series. This information, never reported to date for the full nickelate family, is complementary to that obtained from neutron diffraction, which probes the moment values in the magnetically ordered state.

For the nickelates without magnetic RE cations (RE = Y, Lu), $1/\chi$ was modelled with a Curie-Weiss law $\frac{1}{\chi} = \frac{T-\theta}{C_{\text{Ni}}}$, where θ is the Curie-Weiss temperature and C_{Ni} is the Curie constant, related to the spin-only Ni effective paramagnetic moment

μ_{eff} through the expression $\mu_{\text{eff}} = \sqrt{\frac{3k_B C_{\text{Ni}}}{N_A \mu_B^2}} \sim 2.828 \sqrt{C_{\text{Ni}}}$. Here,

k_B is the Boltzmann constant, N_A is the Avogadro number, and μ_B is the Bohr magneton. The obtained μ_{eff} values were then compared with those reported in neutron diffraction studies. In the case of YNiO_3 , the paramagnetic moments of the Ni at the ‘‘large’’ and ‘‘small’’ octahedral sites reported in ref.²⁴ are $1.4 \mu_B$ and $0.6 \mu_B$. These values are respectively smaller and larger than those of Ni^{2+} ($t_{2g}^6 e_g^2$, $2 \mu_B$) and Ni^{4+} ($t_{2g}^6 e_g^0$, $0 \mu_B$), which, in a simple ionic picture, was interpreted as a signature of partial Ni charge disproportionation. From the Curie fits of our YNiO_3 and LuNiO_3 samples (Figure 7) we obtain $\mu_{\text{eff}} = 2.62 \mu_B$ (Y) and $2.96 \mu_B$ (Lu). For YNiO_3 , this value is very close to the one expected for the degree of disproportionation determined from neutron diffraction ($\mu_{\text{eff}} = 2.51 \mu_B$), and much larger than the effective paramagnetic moment of non-disproportionated Ni^{3+} LS ($\mu_{\text{eff}} = 1.73 \mu_B$). At the same level of approximation, this suggests that the moments (and the charges) of both Ni sites remain different in the paramagnetic region close of T_N , with a degree of disproportionation similar to that observed in the antiferromagnetic state. Another interesting result is the high value of the Curie-Weiss temperatures, $\theta = -245$ K (Y) and -500 K (Lu), which indicate the presence of large, predominantly antiferromagnetic interactions in the Ni sublattice. The Ramirez ratios, $|\theta|/T_N = 1.60$ (Y) and 3.96 (Lu), also suggest the existence of weak magnetic frustration, which increases as the RE ionic radii decrease.

For the nickelates with RE = Pr, Nd, Gd, Dy, Ho and Er, the $\chi(T)$ curves are dominated by the paramagnetic signal of the RE^{3+} cations. Given the impossibility of extracting the Ni

contribution independently, we carried out the Curie-Weiss fits by assuming the simultaneous presence of Ni^{3+} LS with spin-only moment ($\mu_{\text{eff}} = 1.73 \mu_B$). $1/\chi$ was thus modelled with a Curie-Weiss law $\frac{1}{\chi} = \frac{T-\theta}{C}$, where $C = C_{\text{RE}} + C_{\text{Ni}}$ is the fitted Curie constant, θ is the Curie-Weiss temperature, $C_{\text{Ni}} = 0.375 \text{ emu K mol}^{-1}$ is the Ni contribution, and C_{RE} the contribution of the RE cation.

The μ_{eff} values obtained in this way are 3.583 (Pr), 3.798 (Nd), 8.938 (Gd), 11.94 (Dy), 10.95 (Ho), and $9.704 \mu_B$ (Er), which, as expected, are slightly larger than the nominal free-ion values (Table S3). The Curie-Weiss temperatures, θ , are -76.2 (Pr), -102.8 (Nd), -12.8 (Gd), -10.1 (Dy), -35.0 (Ho), and -20.2 K (Er). As in the case of the Ni-Ni coupling, the dominant magnetic interactions when both Ni and a magnetic RE cation are present are also antiferromagnetic, but with significantly smaller values.

For SmNiO_3 and EuNiO_3 , the smaller energy separation between the ground and the first excited J -multiplets of the RE^{3+} cations results in some admixture of the excited state in the ground state, giving rise to an additional van Vleck-type contribution to the paramagnetic response. The Curie-Weiss law is no longer obeyed in the full paramagnetic state, and if used at sufficiently high temperatures, leads in general to μ_{eff} values larger than the single-ion values and high Curie-Weiss temperatures, suggesting the presence unrealistically large exchange interactions.⁶⁰ For Sm^{3+} , with an odd number of $4f$ electrons, the lowest-lying J multiplets (${}^6H_{5/2}$ and ${}^6H_{7/2}$) are split by the CEF interaction into three and four Kramers doublets, respectively. The energy separation between the lowest-lying doublet of the ground state and that of the first excited multiplet, as determined from inelastic neutron scattering, is 132 meV ($\sim 1530 \text{ K}$).³³

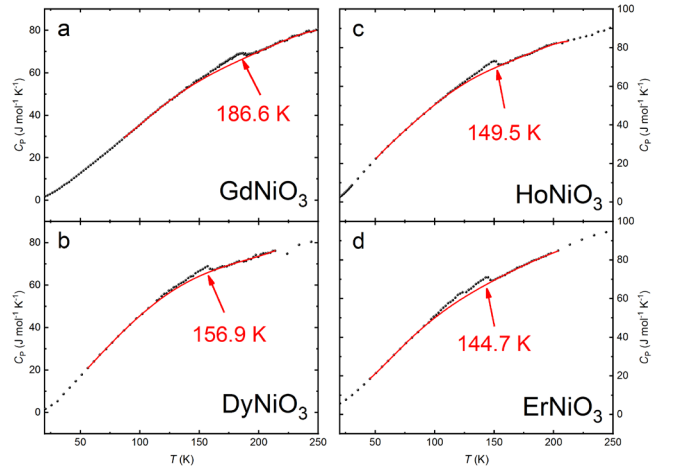


Figure 8. Temperature dependence of the heat capacity for the GdNiO_3 , DyNiO_3 , HoNiO_3 and ErNiO_3 single crystals. The red lines represent the phonon contribution estimates as described in the Methods section (SI).

The doublets of ${}^6H_{7/2}$ are thus expected to be partially populated below $T_N = 218.2$ K, the temperature above which both Ni^{3+} and Sm^{3+} are paramagnetic. This is confirmed by the results of the Curie-Weiss fits, which lead to $\mu_{\text{eff}} = 5.63 \mu_B$, a value that is much larger than the free ion value ($0.85 \mu_B$), and a very large $\theta = -1035.9$ K. In the case of Eu^{3+} , with an

even number of $4f$ electrons, the lowest-lying J multiplets are the singlet 7F_0 and triplet 7F_1 states. The ground state is not degenerate and the energy gap with the lowest-lying level of 7F_1 is only 34.5 meV (~ 400 K).⁶¹ The admixture between ground and excited states is thus expected to be much more important than in the case of Sm^{3+} . This is supported by the shape of the $\chi(T)$ curve, where the characteristic, temperature-independent van Vleck contribution is clearly observed below ~ 100 K (blue arrow in the EuNiO_3 panel of Figure 7). A small paramagnetic contribution is also present at lower temperatures, which we tentatively attribute to an unidentified paramagnetic impurity. As in the case of Sm^{3+} , a Curie-Weiss fit between T_N and 300 K led to $\mu_{\text{eff}} = 5.46 \mu_B$, which is much higher than the free ion value ($0 \mu_B$), and a large $\theta = -371$ K.

Entropy loss associated with the antiferromagnetic order of the Ni magnetic moments. A further parameter providing information about the Ni magnetic moment is the the entropy loss ΔS associated with the Ni cooperative order below T_N . For the nickelates with RE = Gd, Dy, Ho and Er, ΔS was estimated from the excess C_p after subtraction of the phonon contribution (red curves in Fig. 8, see the SI Methods section in the SI for details). The obtained entropy changes ΔS were 580, 566, 594 and 1052 $\text{mJ mol}^{-1} \text{K}^{-1}$ for RE = Gd, Dy, Ho and Er, respectively. These values were then compared with the theoretical value expected from the ordering of Ni^{3+} magnetic moments with $S = \frac{1}{2} (\Delta S = R \ln 2 = 0.69 R)$, where R is the ideal gas constant. For our nickelates we obtain $\Delta S \sim 0.070 R$ (Gd), $0.068 R$ (Dy), $0.071 R$ (Ho) and $0.127 R$ (Er). These values differ slightly from those reported by Alonso et al.¹³ ($\sim 0.022 R$ and $\sim 0.090 R$ for RE = Gd and Dy, respectively), although the discrepancy might be due to the smallness of the anomaly and the details of the phonon background subtraction. In any case, both our ΔS values and those of ref.¹³ are much lower than the theoretical value of $0.69 R$. Similar observations have been reported for SmNiO_3 ($\Delta S = 0.03 R$),⁶² and even for NdNiO_3 ($\Delta S = 0.12 R$)⁶³ and PrNiO_3 ($\Delta S = 0.16 R$),³² where the magnetic, electronic and structural transitions coincide and extra contributions to ΔS would be expected. Although the entropy jump is indeed larger for these two nickelates, it is still far below the purely magnetic theoretical value. This suggests the existence of “lost” magnetic entropy above T_N for the whole RENiO_3 family, most probably in the form of magnetic correlations that, in the case of PrNiO_3 and NdNiO_3 , could survive even in the metallic phase above $T_N = T_{\text{MIT}}$.

CONCLUSIONS

To summarize, we have reported the first successful growth of phase-pure RENiO_3 single crystals with RE = Nd, Sm, Gd, Dy, Y, Ho, Er and Lu. The crystals have well-defined facets, regular, slightly truncated prismatic habit and sizes up to $\sim 75 \mu\text{m}$. We used an original method involving the use of a highly reactive molten salts flux, a high temperature gradient and oxygen gas pressures up to 2000 bar, delivered by an unique, non-commercial apparatus recently installed at the PSI. This technically challenging route involves the use of oxygen gas pressure five times larger than those employed in previous studies ($P_{\text{max}} \sim 400$ bar), but ten times lower than the 20 kbar required to synthesize ceramics with RE = Dy to Lu

using hydrostatic pressure. Moreover, the large size of the reactor allows the preparation of material amounts up to 10 times larger than in the case of hydrostatic pressure. The availability of these samples enabled the first systematic investigation of RENiO_3 bulk magnetic properties. This provided novel information on the evolution of the dominant magnetic interactions and the magnetic correlations in the paramagnetic phase along the series, and the first experimental determination of T_N for ErNiO_3 .

The nickelate single crystals reported in this study are unique in many senses. On one side, they are the first-ever RENiO_3 perovskites with RE = Sm, Gd, Dy, Y, Ho, Er and Lu grown in single crystalline form. On the other, their metal-to-insulator and antiferromagnetic transition temperatures are identical to those reported so far for ceramic samples. This matching will allow to complete the existing body of experimental information on ceramic samples (used in theoretical studies during the last 20 years) with novel, but perfectly compatible data. Complex measurements never conducted to date will become now possible, as long as the employed techniques are compatible with the crystal size. This includes Focused Ion Beam techniques, which could be used in combination with transport and magnetic measurements to investigate the anisotropy of basic physical properties, presently unknown for the full nickelate family. X-ray spectroscopies such as Angle-Resolved X-ray Photoemission or Inelastic X-ray Scattering (resonant and non-resonant) could take advantage of the tiny synchrotron X-ray beam cross sections to probe the electronic, phonon and magnon dispersion curves. Such measurements, out of the scope of this work, should provide crucial information for theoreticians and help to improve the models, fundamental energies and methods for describing the complex physics of these materials. It should also contribute to a better understanding of the complex region at the boundary between localized and itinerant behavior, and to the elaboration of design strategies, which might lead to novel transition metal oxides with improved, societally relevant functional properties.

ASSOCIATED CONTENT

Supporting Information

Materials, crystallographic methods, Scanning Electron Microscopy, magnetization, heat capacity, differential scanning calorimetry, phase identification for YbNiO_3 and TmNiO_3 , optical microscope images, REClO impurity analysis, Elemental analysis, SmClO recrystallization, Rietveld fits, RT crystal structures, tables with lattice parameters, atomic positions, reliability factors, angles, tilts, distances, Néel and Metal-Insulator transition temperatures, Curie constants, effective magnetic moments and Curie-Weiss temperatures.

Accession codes

CCDC 2077728-2077729 and 2077640-2077642 contain the supplementary crystallographic data for this paper.

AUTHOR INFORMATION

Author Contributions

D.J.G.: Synthesized the all samples, except EuNiO_3 and PrNiO_3 , synthesized respectively by P.L and Y.M.K.; M.K. measured the SEM and provided the EDX analysis; D.J.G, Y.M.K and M.M. conducted physical properties and PXRD measurements and analyzed the data; D.J.G, Y.M.K and T.L. measured, solved and refined the single crystal structures; M.M. wrote the manuscript with input from all authors. All authors have given approval to the final version of the manuscript.

Funding Sources

This work was supported by the Swiss National Science Foundation through the NCCR MARVEL (Grant No. 51NF40-182892), and the R'equip Grant n. 461 206021_139082.

ACKNOWLEDGMENTS

We thank K. Conder, J. Karpinski, A. Hampel, C. Ederer, N. Spaldin, A. Georges, O. Peil, D. van der Marel, J. Tessier, I. Ardizzone, Philip Moll and D. Mazzone for fruitful discussions.

REFERENCES

1. Mott, N. F. The Transition to the Metallic State. *Philos. Mag.* **1961**, *6*, 287-309.
2. Capasso, F. Band-Gap Engineering - from Physics and Materials to New Semiconductor-Devices. *Science* **1987**, *235*, 172-176.
3. Lau, B.; Millis, A. J. Theory of the Magnetic and Metal-Insulator Transitions in RNiO_3 Bulk and Layered Structures. *Phys. Rev. Lett.* **2013**, *110*, 126404.
4. Mazin, I. I.; Khomskii, D. I.; Lengsdorf, R.; Alonso, J. A.; Marshall, W. G.; Ibberson, R. M.; Podlesnyak, A.; Martínez-Lope, M. J.; Abd-Elmeguid, M. M. Charge Ordering as Alternative to Jahn-Teller Distortion. *Phys. Rev. Lett.* **2007**, *98*, 176406.
5. Lee, S.; Chen, R.; Balents, L. Landau Theory of Charge and Spin Ordering in the Nickelates. *Phys. Rev. Lett.* **2011**, *106*, 016405.
6. Peil, O. E.; Hampel, A.; Ederer, C.; Georges, A. Mechanism and control parameters of the coupled structural and metal-insulator transition in nickelates. *Phys. Rev. B* **2019**, *99*, 245127.
7. Mercy, A.; Bieder, J.; Iniguez, J.; Ghosez, P. Structurally triggered metal-insulator transition in rare-earth nickelates. *Nat. Commun.* **2017**, *8*, 1677.
8. Medarde, M. L. Structural, magnetic and electronic properties of perovskites (R = rare earth). *J. Phys-Condens. Mat.* **1997**, *9*, 1679-1707.
9. Goodenough, J. B.; Mott, N. F.; Pouchard, M.; Demazeau, G.; Hagenmuller, P. Comparative Study on Magnetic Behavior of LaNiO_3 and LaCuO_3 Phases. *Mater. Res. Bull.* **1973**, *8*, 647-655.
10. García-Muñoz, J. L.; Rodríguez-Carvajal, J.; Lacorre, P.; Torrance, J. B. Neutron-diffraction study of RNiO_3 (R=La,Pr,Nd,Sm): Electronically induced structural changes across the metal-insulator transition. *Phys. Rev. B* **1992**, *46*, 4414-4425.
11. Lacorre, P.; Torrance, J. B.; Pannetier, J.; Nazzal, A. I.; Wang, P. W.; Huang, T. C. Synthesis, crystal structure, and properties of metallic PrNiO_3 : Comparison with metallic NdNiO_3 and semiconducting SmNiO_3 . *J. Solid State Chem.* **1991**, *91*, 225-237.
12. Alonso, J. A.; Martínez-Lope, M. J.; Rasines, I. Preparation, Crystal Structure, and Metal-to-Insulator Transition of EuNiO_3 . *J. Solid State Chem.* **1995**, *120*, 170-174.
13. Alonso, J. A.; Martínez-Lope, M. J.; Casais, M. T.; Martínez, J. L.; Demazeau, G.; Largeteau, A.; García-Muñoz, J. L.; Muñoz, A.; Fernández-Díaz, M. T. High-pressure preparation, crystal structure, magnetic properties, and phase transitions in GdNiO_3 and DyNiO_3 perovskites. *Chem. Mater.* **1999**, *11*, 2463-2469.
14. Alonso, J. A.; Martínez-Lope, M. J.; Casais, M. T.; Aranda, M. A. G.; Fernández-Díaz, M. T. Metal-Insulator Transitions, Structural and Microstructural Evolution of RNiO_3 (R = Sm, Eu, Gd, Dy, Ho, Y) Perovskites: Evidence for Room-Temperature Charge Disproportionation in Monoclinic HoNiO_3 and YNiO_3 . *J. Am. Chem. Soc.* **1999**, *121*, 4754-4762.
15. Alonso, J. A.; Martínez-Lope, M. J.; Casais, M. T.; García-Muñoz, J. L.; Fernández-Díaz, M. T.; Aranda, M. A. G. High-temperature structural evolution of RNiO_3 (R=Ho, Y, Er, Lu) perovskites: Charge disproportionation and electronic localization. *Phys. Rev. B* **2001**, *64*, 094102.
16. Alonso, J. A.; Martínez-Lope, M. J.; Presniakov, I. A.; Sobolev, A. V.; Rusakov, V. S.; Gapochka, A. M.; Demazeau, G.; Fernández-Díaz, M. T. Charge disproportionation in RNiO_3 (R=Tm, Yb) perovskites observed in situ by neutron diffraction and 57Fe probe Mössbauer spectroscopy. *Phys. Rev. B* **2013**, *87*, 184111.
17. Torrance, J. B.; Lacorre, P.; Nazzal, A. I.; Ansaldo, E. J.; Niedermayer, C. Systematic study of insulator-metal transitions in perovskites RNiO_3 (R=Pr,Nd,Sm, Eu) due to closing of charge-transfer gap. *Phys. Rev. B* **1992**, *45*, 8209-8212.
18. Rodríguez-Carvajal, J.; Rosenkranz, S.; Medarde, M.; Lacorre, P.; Fernández-Díaz, M. T.; Fauth, F.; Trounov, V. Neutron-diffraction study of the magnetic and orbital ordering in 154SmNiO_3 and 153EuNiO_3 . *Phys. Rev. B* **1998**, *57*, 456-464.
19. Demazeau, G.; Marbeuf, A.; Pouchard, M.; Hagenmuller, P. Sur une série de composés oxygènes du nickel trivalent dérivés de la perovskite. *J. Solid State Chem.* **1971**, *3*, 582-589.
20. Fernández-Díaz, M. T.; Alonso, J. A.; Martínez-Lope, M. J.; Casais, M. T.; García-Muñoz, J. L. Magnetic structure of the HoNiO_3 perovskite. *Phys. Rev. B* **2001**, *64*, 144417.
21. Kim, S. J.; Martínez-Lope, M. J.; Fernández-Díaz, M. T.; Alonso, J. A.; Presniakov, I.; Demazeau, G. Evidence of Ni(III) Disproportionation in the TiNiO_3 Perovskite Lattice through Neutron Powder Diffraction and Mössbauer Spectroscopy. *Chem. Mat.* **2002**, *14*, 4926-4932.
22. Korosec, L.; Pikulski, M.; Shiroka, T.; Medarde, M.; Luetkens, H.; Alonso, J. A.; Ott, H. R.; Mesot, J. New magnetic phase in the nickelate perovskite TiNiO_3 . *Phys. Rev. B* **2017**, *95*, 060411.
23. Medarde, M.; Lacorre, P.; Conder, K.; Fauth, F.; Furrer, A. Giant O-16-O-18 isotope effect on the metal-insulator transition of RNiO_3 perovskites (R equals rare earth). *Phys. Rev. Lett.* **1998**, *80*, 2397-2400.
24. Alonso, J. A.; García-Muñoz, J. L.; Fernández-Díaz, M. T.; Aranda, M. A. G.; Martínez-Lope, M. J.; Casais, M. T. Charge Disproportionation in RNiO_3 Perovskites: Simultaneous Metal-Insulator and Structural Transition in YNiO_3 . *Phys. Rev. Lett.* **1999**, *82*, 3871-3874.
25. Medarde, M.; Fernández-Díaz, M. T.; Lacorre, P. Long-range charge order in the low-temperature insulating phase of PrNiO_3 . *Phys. Rev. B* **2008**, *78*, 212101.
26. Alonso, J. A.; Martínez-Lope, M. J.; Demazeau, G.; Fernández-Díaz, M. T.; Presniakov, I. A.; Rusakov, V. S.; Gubaidulina, T. V.; Sobolev, A. V. On the evolution of the DyNiO_3 perovskite across the metal-insulator transition through neutron

- diffraction and Mossbauer spectroscopy studies. *Dalton Trans.* **2008**, 6584-6592.
27. Serrano-Sánchez, F.; Fauth, F.; Martínez, J. L.; Alonso, J. A. Experimental Observation of Monoclinic Distortion in the Insulating Regime of SmNiO₃ by Synchrotron X-ray Diffraction. *Inorg. Chem.* **2019**, *58*, 11828-11835.
 28. Garcia-Munoz, J. L.; Aranda, M. A. G.; Alonso, J. A.; Martinez-Lope, M. J. Structure and charge order in the antiferromagnetic band-insulating phase of NdNiO₃. *Phys. Rev. B* **2009**, *79*, 134432.
 29. Johnston, S.; Mukherjee, A.; Elfimov, I.; Berciu, M.; Sawatzky, G. A. Charge Disproportionation without Charge Transfer in the Rare-Earth-Element Nickelates as a Possible Mechanism for the Metal-Insulator Transition. *Phys. Rev. Lett.* **2014**, *112*, 106404.
 30. Vobornik, I.; Perfetti, L.; Zacchigna, M.; Grioni, M.; Margaritondo, G.; Mesot, J.; Medarde, M.; Lacorre, P. Electronic-structure evolution through the metal-insulator transition in RNiO₃. *Phys. Rev. B* **1999**, *60*, R8426-R8429.
 31. Ruppen, J.; Teyssier, J.; Ardizzone, I.; Peil, O. E.; Catalano, S.; Gibert, M.; Triscone, J. M.; Georges, A.; van der Marel, D. Impact of antiferromagnetism on the optical properties of rare-earth nickelates. *Phys. Rev. B* **2017**, *96*, 045120.
 32. Gawryluk, D. J.; Klein, Y. M.; Shang, T.; Sheptyakov, D.; Keller, L.; Casati, N.; Lacorre, P.; Fernández-Díaz, M. T.; Rodríguez-Carvajal, J.; Medarde, M. Distortion mode anomalies in bulk PrNiO₃: Illustrating the potential of symmetry-adapted distortion mode analysis for the study of phase transitions. *Phys. Rev. B* **2019**, *100*, 205137.
 33. Rosenkranz, S.; Medarde, M.; Fauth, F.; Mesot, J.; Zolliker, M.; Furrer, A.; Staub, U.; Lacorre, P.; Osborn, R.; Eccleston, R. S.; Trounov, V. Crystalline electric field of the rare-earth nickelates RNiO₃ (R = Pr, Nd, Sm, Eu, and Pr_{1-x}La_x, 0 ≤ x ≤ 0.7) determined by inelastic neutron scattering. *Phys. Rev. B* **1999**, *60*, 14857-14867.
 34. Shannon, R. Revised effective ionic radii and systematic studies of interatomic distances in halides and chalcogenides. *Acta Crystallogr. A* **1976**, *32*, 751-767.
 35. Jones, R. O.; Gunnarsson, O. The Density Functional Formalism, Its Applications and Prospects. *Rev. Mod. Phys.* **1989**, *61*, 689-746.
 36. Georges, A.; Kotliar, G.; Krauth, W.; Rozenberg, M. J. Dynamical mean-field theory of strongly correlated fermion systems and the limit of infinite dimensions. *Rev. Mod. Phys.* **1996**, *68*, 13-125.
 37. Dhaka, R. S.; Das, T.; Plumb, N. C.; Ristic, Z.; Kong, W.; Matt, C. E.; Xu, N.; Dolui, K.; Razzoli, E.; Medarde, M.; Patthey, L.; Shi, M.; Radovic, M.; Mesot, J. Tuning the metal-insulator transition in NdNiO₃ heterostructures via Fermi surface instability and spin fluctuations. *Phys. Rev. B* **2015**, *92*, 035127.
 38. Cappelli, E.; Tromp, W. O.; Walker, S. M.; Tamai, A.; Gibert, M.; Baumberger, F.; Bruno, F. Y. A laser-ARPES study of LaNiO₃ thin films grown by sputter deposition. *Appl. Mater.* **2020**, *8*, 051102.
 39. Catalan, G. Progress in perovskite nickelate research. *Phase Transit.* **2008**, *81*, 729-749.
 40. Catalano, S.; Gibert, M.; Fowlie, J.; Íñiguez, J.; Triscone, J. M.; Kreisel, J. Rare-earth nickelates RNiO₃: thin films and heterostructures. *Rep. Prog. Phys.* **2018**, *81*, 046501.
 41. Lu, Y.; Betto, D.; Fursich, K.; Suzuki, H.; Kim, H. H.; Cristiani, G.; Logvenov, G.; Brookes, N. B.; Benckiser, E.; Haverkort, M. W.; Khaliullin, G.; Le Tacon, M.; Minola, M.; Keimer, B. Site-Selective Probe of Magnetic Excitations in Rare-Earth Nickelates Using Resonant Inelastic X-ray Scattering. *Phys. Rev. X* **2018**, *8*, 031014.
 42. Fursich, K.; Lu, Y.; Betto, D.; Bluschke, M.; Porras, J.; Schierle, E.; Ortiz, R.; Suzuki, H.; Cristiani, G.; Logvenov, G.; Brookes, N. B.; Haverkort, M. W.; Le Tacon, M.; Benckiser, E.; Minola, M.; Keimer, B. Resonant inelastic x-ray scattering study of bond order and spin excitations in nickelate thin-film structures. *Phys. Rev. B* **2019**, *99*, 165124.
 43. Prakash, J.; Blakely, C. K.; Poltavets, V. V. Low temperature high-pressure synthesis of LnNiO₃ (Ln = Eu, Gd) in molten salts. *Solid State Sci.* **2013**, *17*, 72-75.
 44. Zhou, J. S.; Goodenough, J. B.; Dabrowski, B. Structure anomaly and electronic transition in RNiO₃ (R=La,Pr,...,Gd). *Phys. Rev. B* **2004**, *70*, 081102.
 45. Chen, J. K.; Li, Z.; Dong, H. L.; Xu, J. N.; Wang, V.; Feng, Z. J.; Chen, Z. Q.; Chen, B.; Chen, N. F.; Mao, H. K. Pressure induced unstable electronic states upon correlated nickelates metastable perovskites as batch synthesized via heterogeneous nucleation. *Adv. Funct. Mater.* **2020**, *30*, 2000987.
 46. Escote, M. T.; da Silva, A. M. L.; Matos, J. R.; Jardim, R. F. General properties of polycrystalline LnNiO₃ (Ln = Pr, Nd, Sm) compounds prepared through different precursors. *J. Solid State Chem.* **2000**, *151*, 298-307.
 47. Alonso, J. A.; Martínez-Lope, M. J.; Casais, M. T.; García-Muñoz, J. L.; Fernández-Díaz, M. T. Room-temperature monoclinic distortion due to charge disproportionation in RNiO₃ perovskites with small rare-earth cations (R = Ho, Y, Er, Tm, Yb, and Lu): A neutron diffraction study. *Phys. Rev. B* **2000**, *61*, 1756-1763.
 48. Saito, T.; Azuma, M.; Nishibori, E.; Takata, M.; Sakata, M.; Nakayama, N.; Arima, T.; Kimura, T.; Urano, C.; Takano, M. Monoclinic distortion in the insulating phase of PrNiO₃. *Physica B* **2003**, *329*, 866-867.
 49. Alonso, J. A.; Muñoz, A.; Largeteau, A.; Demazeau, G. Crystal growth of NdNiO₃ perovskite under high oxygen pressure. *J. Phys-Condens. Mat.* **2004**, *16*, S1277-S1281.
 50. Alonso, J. A.; Demazeau, G.; Largeteau, A.; Kurowski, D.; Hoffmann, R. D.; Pottgen, R. Crystal structure of NdNiO₃ at 123 and 292 K. *Z. Naturforsch. B* **2006**, *61*, 346-349.
 51. Lorenzo, J. E.; Hodeau, J. L.; Paololini, L.; Le Floch, S.; Alonso, J. A.; Demazeau, G. Resonant x-ray scattering experiments on electronic orderings in NdNiO₃ single crystals. *Phys. Rev. B* **2005**, *71*, 045128.
 52. Zhang, J.; Zheng, H.; Ren, Y.; Mitchell, J. F. High-Pressure Floating-Zone Growth of Perovskite Nickelate LaNiO₃ Single Crystals. *Cryst. Growth Des* **2017**, *17*, 2730-2735.
 53. Guo, H.; Li, Z. W.; Zhao, L.; Hu, Z.; Chang, C. F.; Kuo, C. Y.; Schmidt, W.; Piovano, A.; Pi, T. W.; Sobolev, O.; Khomskii, D. I.; Tjeng, L. H.; Komarek, A. C. Antiferromagnetic correlations in the metallic strongly correlated transition metal oxide LaNiO₃. *Nat. Commun.* **2018**, *9*, 43.
 54. Zheng, H.; Zhang, J.; Wang, B.; Phelan, D.; Krogstad, M. J.; Ren, Y.; Phelan, W. A.; Chmaissem, O.; Poudel, B.; Mitchell, J. F. High pO₂ Floating Zone Crystal Growth of the Perovskite Nickelate PrNiO₃. *Crystals* **2019**, *9*, 324.
 55. Zheng, H.; Wang, B. X.; Phelan, D.; Zhang, J. J.; Ren, Y.; Krogstad, M. J.; Rosenkranz, S.; Osborn, R.; Mitchell, J. F. Oxygen Inhomogeneity and Reversibility in Single Crystal LaNiO₃-d. *Crystals* **2020**, *10*, 557.
 56. Karpinski, J. High pressure in the synthesis and crystal growth of superconductors and III-N semiconductors. *Philos. Mag.* **2012**, *92*, 2662-2685.
 57. Medarde, M.; Dallera, C.; Grioni, M.; Delley, B.; Vernay, F.; Mesot, J.; Sikora, M.; Alonso, J. A.; Martinez-Lope, M. J. Charge disproportionation in RNiO₃ perovskites (R=rare earth) from high-resolution x-ray absorption spectroscopy. *Phys. Rev. B* **2009**, *80*, 245105.
 58. Varignon, J.; Grisolia, M. N.; Iniguez, J.; Barthelemy, A.; Bibes, M. Complete phase diagram of rare-earth nickelates from first-principles. *Npj Quantum Mater.* **2017**, *2*, 21.
 59. Subedi, A.; Peil, O. E.; Georges, A. Low-energy description of the metal-insulator transition in the rare-earth nickelates. *Phys. Rev. B* **2015**, *91*, 075128.

60. Takikawa, Y.; Ebisu, S.; Nagata, S. Van Vleck paramagnetism of the trivalent Eu ions. *J. Phys. Chem. Solids* **2010**, *71*, 1592-1598.
61. Rosenkranz, S.; Staub, U.; Furrer, A.; Osborn, R.; Lacorre, P.; Trounov, V. Intermultiplet crystal field transitions in EuNiO_3 . *J. Alloy. Compd.* **1997**, *250*, 577-580.
62. Perez-Cacho, J.; Blasco, J.; Garcia, J.; Castro, M.; Stankiewicz, J. Study of the phase transitions in SmNiO_3 . *J. Phys-Condens. Mat.* **1999**, *11*, 405-415.
63. Perez, J.; Stankiewicz, J.; Blasco, J.; Castro, M.; Garcia, J. The metal-insulator transition in $\text{NdNi}_{1-x}\text{Cu}_x\text{O}_3$ perovskites. *J. Phys-Condens. Mat.* **1996**, *8*, 10393-10405.